

Parametrization of F_2^γ at low Q^2 and of $\sigma_{\gamma\gamma}$ and $\sigma_{\gamma^*\gamma}$ at high energies

B. Badełek,¹ M. Krawczyk,² J. Kwieciński,³ and A. M. Staśto³

¹*Department of Physics, Uppsala University, P.O. Box 530, 751 21 Uppsala, Sweden*
 and *Institute of Experimental Physics, Warsaw University, 00-681 Warsaw, Poland*

²*Institute of Theoretical Physics, Warsaw University, 00-681 Warsaw, Poland*

³*Department of Theoretical Physics, H. Niewodniczański Institute of Nuclear Physics, 31-342 Cracow, Poland*

(Received 18 January 2000; revised manuscript received 19 May 2000; published 12 September 2000)

A parametrization of the real photon structure function F_2^γ in the low Q^2 , low x region is formulated. It includes both the vector meson dominance (VMD) and the QCD components, the latter suitably extrapolated to the low Q^2 region and based on arbitrary parton distributions in the photon. The parametrization used together with the Gluck, Reya, and Vogt (GRV) and Gluck, Reya, and Schienbein (GRS) parton densities describes reasonably well the existing high energy data on F_2^γ , $\sigma_{\gamma\gamma}$, and the low Q^2 data on $\sigma_{\gamma^*\gamma}$. Predictions for $\sigma_{\gamma\gamma}$ and for $\sigma_{\gamma^*\gamma}$ for energies which may become accessible in future linear colliders are also given.

PACS number(s): 13.60.Hb, 12.38.Bx, 12.40.Vv, 14.70.Bh

I. INTRODUCTION

Electron-photon scattering,

$$e\gamma \rightarrow \gamma^*\gamma \rightarrow \text{hadrons}, \quad (1)$$

studied in high energy e^+e^- collisions with a tagged electron is an analogue of inelastic lepton-nucleon scattering. Here the probe, a virtual photon of four momentum q ($q^2 = -Q^2 < 0$), tests the target particle, the real photon of four momentum p ($p^2 = 0$). The corresponding spin averaged cross section, Fig. 1, can be parametrized, e.g., by the photon structure functions $F_1^\gamma(x, Q^2)$ and $F_2^\gamma(x, Q^2)$. The Bjorken parameter x is conventionally defined as $x = Q^2/(2p \cdot q)$. Thus the process, Eq. (1) permits an insight into the inner structure of the real photon.

At large Q^2 the photon structure function is described by perturbative QCD [1–5]. However in the low Q^2 region, $Q^2 \lesssim 1 \text{ GeV}^2$, it is expected that the vector meson dominance (VMD) contribution [6] is important.

In this paper we present a model of the photon structure function F_2^γ which includes both the VMD contribution and the QCD term, suitably extrapolated to the low Q^2 region. This approach is based on the extension of a similar representation of the nucleon structure function [7–9] to the case of the photon. Possible parametrizations of the photon structure function, which extend to the low Q^2 region, have also been discussed in Refs. [10–12]. The parametrization proposed in Ref. [10] is based upon the quark parton model supplemented by the contribution from the hadronic structure of the photon. The energy dependence of the latter has a Regge form. The Q^2 dependence is parametrized in terms of the simple form factors which, if combined with the Regge-type energy dependence, generate at large Q^2 the Bjorken scaling behavior of the corresponding part of the structure function. In Ref. [11] the energy dependence of the cross section is also parametrized in a Regge-like form with the Q^2 dependence specified by the suitable form factors which contain terms corresponding to the VMD contribution. The parametrization discussed in Ref. [12] is based upon a model corresponding to the interaction of color dipoles, i.e., the $q\bar{q}$

pairs into which the photon(s) fluctuate. In our approach the contribution coming from the light vector mesons within the VMD model is similar to that used by other authors (see e.g. Ref. [11]) although the details concerning an estimate of the relevant total cross sections are slightly different. The novel feature of our model is the treatment of the contribution coming from high masses of the hadronic states which couple to the virtual photons. In our scheme this contribution is directly related to the photon structure function in the large Q^2 region. The low and high mass hadronic states are separated at Q_0 , a parameter whose value was taken to be identical to that for the F_2^p .

Our framework permits us to describe the $\gamma\gamma$ and $\gamma^*\gamma$ total cross sections as functions of energy. The energy dependence of $\sigma_{\gamma\gamma}$ is also described by other models, [11–18]. Most of them incorporate the Regge-like parametrization of the total $\gamma\gamma$ cross sections; some provide a detailed insight into the structure of final states and a decomposition of the $\gamma\gamma$ total cross section into terms corresponding to the appropriate subdivision of photon interactions and event classes [11,14]. The possibility that part of the $\gamma\gamma$ cross section is driven by the production of minijets has been discussed in

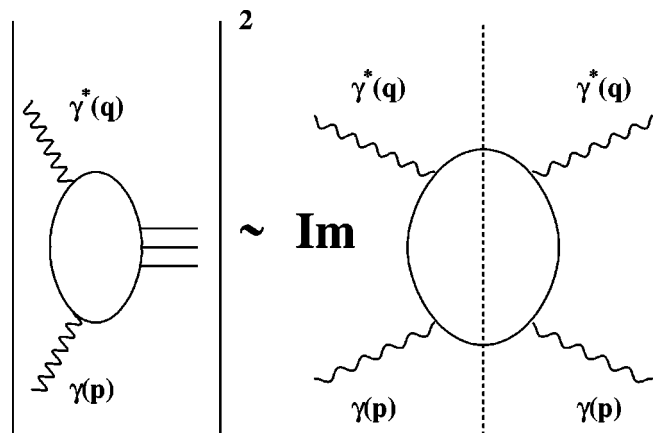


FIG. 1. The cross section for the $\gamma^*\gamma \rightarrow \text{hadrons}$ scattering and its relation to the imaginary part of the forward $\gamma^*\gamma \rightarrow \gamma^*\gamma$ amplitude.

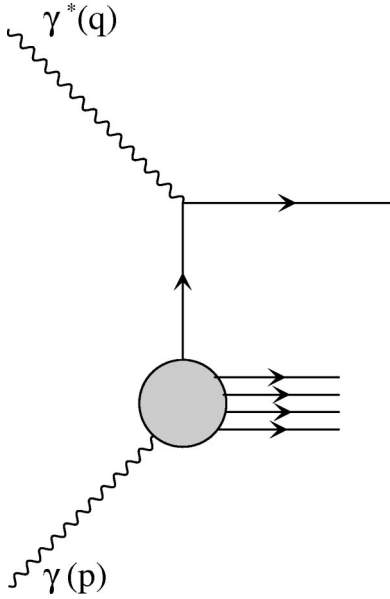


FIG. 2. $\gamma^*\gamma$ scattering as a mechanism for probing partonic structure of the real photon.

[13,16]. Certain approaches analyze the behavior of the cross sections on the virtualities of both interacting photons [11,12,15,17,18].

The content of our paper is as follows: In Sec. II we recall the QCD description of the photon structure functions and in Sec. III we briefly describe the VMD model in the process $\gamma^*\gamma \rightarrow \text{hadrons}$. In Sec. IV we present a parametrization of the photon structure function, as well as the total cross section for the interaction of two real photons and of the virtual and real photon. In Sec. V we compare our theoretical predictions with the experimental data on the F_2^γ and on the total cross sections $\sigma_{\gamma\gamma}$ and $\sigma_{\gamma^*\gamma}$. We also give predictions for $\sigma_{\gamma\gamma}$ in the very high energy range which can become accessible in future linear colliders. Finally in Sec. VI we give the summary of our results.

II. PARTONIC CONTENT OF THE PHOTON

In the large Q^2 , i.e., in the deep inelastic limit the virtual photon probes the quark (antiquark) structure of the (real) photon in analogy to the deep inelastic lepton–hadron scattering, Fig. 2. The corresponding photon structure function $F_2^\gamma(x, Q^2)$ may thus be related to quark and antiquark distributions $q_i^\gamma(x, Q^2), \bar{q}_i^\gamma(x, Q^2)$ in the photon

$$F_2^\gamma(x, Q^2) = x \sum_i e_i^2 [q_i^\gamma(x, Q^2) + \bar{q}_i^\gamma(x, Q^2)], \quad (2)$$

where e_i denote the charges of quarks and antiquarks and the sum is over all active quark flavors. To be precise Eq. (2) holds in the leading logarithmic approximation of perturbative QCD. It acquires higher order corrections in next-to-leading approximation and beyond [19,20].

A special feature of the quark structure of the photon with respect to the proton is a possibility of a direct $q\bar{q}$ production

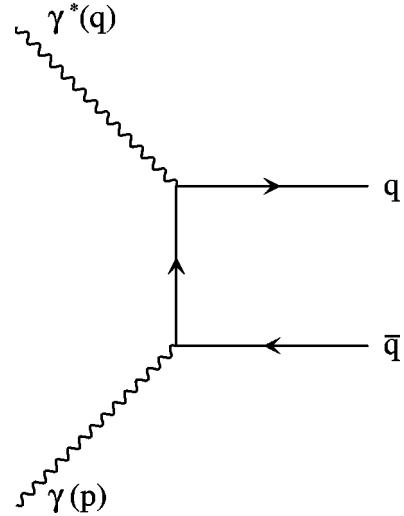


FIG. 3. Diagrammatic representation of the direct $\gamma^*\gamma \rightarrow q\bar{q}$ process.

through the process $\gamma^*\gamma \rightarrow q\bar{q}$, (see Fig. 3), leading to the parton model predictions for the $q_i^\gamma(x, Q^2)$ and $\bar{q}_i^\gamma(x, Q^2)$. A contribution of this process introduces an inhomogeneous term into the equation describing the QCD evolution of the quark (and antiquark) distributions in the photon. The process $\gamma^*\gamma \rightarrow q\bar{q}$ (modified by the QCD evolution) with the pointlike quark coupling both to real and virtual photons dominates in the large Q^2 limit making the photon structure functions exactly calculable in this limit [1,2]. The striking features of these functions are that $F_{1,2}^\gamma$ rises with increasing x at large x , and that $F_{1,2}^\gamma$ shows the scaling violation, $F_{1,2}^\gamma \sim \ln Q^2$.

At low values of x the dominant role in the photon structure functions is played by gluons. The situation here is similar to that of the hadronic structure functions which exhibit a very strong increase with decreasing x , see, e.g., [21]. Those effects are still rather weak in the kinematical region of F_2^γ probed by present experiments but they will be very important in the regime accessible in the future linear e^+e^- ($e\gamma, \gamma\gamma$) colliders [22].

Besides the direct, point-like coupling to quarks, the target photon can fluctuate into vector mesons and other hadronic states which can also have their partonic structure. The latter cannot be calculated perturbatively and thus has to be parametrized phenomenologically [23].

Finally it should be pointed out that the charm quark playing the dominant role in the heavy quark contributions to $F_2^\gamma(x, Q^2)$ is often described just by the lowest order Bethe-Heitler cross section for the process $\gamma^*\gamma \rightarrow c\bar{c}$ and the additional contribution generated by the radiation $g \rightarrow c\bar{c}$ [20,23].

III. DISPERSIVE RELATION FOR $\gamma^*\gamma$ SCATTERING.

F_2^{VMD} AND F_2^{partons} CONTRIBUTIONS TO F_2^γ

The QCD describes the photon structure functions in the large Q^2 region. In the low Q^2 region, however, one expects that the VMD mechanism is important. By the VMD mecha-

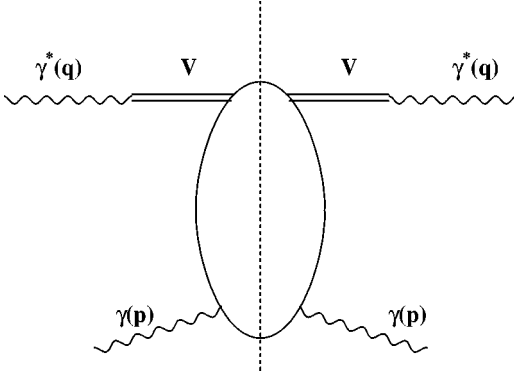


FIG. 4. Diagrammatic representation of the VMD model in the $\gamma^* \gamma$ scattering.

nism in this case we understand the model in which the virtual photon of virtuality Q^2 fluctuates into vector mesons which next undergo interaction with the (real) photon of virtuality $p^2 \approx 0$, (see Fig. 4). In order to be able to describe the photon structure function for arbitrary values of Q^2 it would be very useful to have a unified scheme, which contains both the VMD and the QCD contributions, the latter suitably extended to the region of low values of Q^2 .

This may be achieved by utilizing the dispersive representation in Q^2 of the structure function. To this aim let us notice that the $\gamma^* \gamma$ collision can be viewed as the interaction of a real photon target with a photon with virtuality Q^2 which fluctuates onto a general hadronic state, cf. Fig. 5. We consider the virtual photon first fluctuating onto the $q\bar{q}$ state which next interacts with the real photon. As in the $\gamma^* p$ scattering one can write the dispersion relation for the $\gamma^* \gamma$ scattering as follows [6]:

$$F_2^\gamma(W^2, Q^2) = \frac{Q^2}{4\pi^2\alpha} \sum_q \int \frac{dM^2}{M^2 + Q^2} \int \frac{dM'^2}{M'^2 + Q^2} \times \rho(M^2, M'^2) \frac{1}{W^2} \text{Im} A_{(q\bar{q})-\gamma}(W^2, M^2, M'^2), \quad (3)$$

where M and M' are the invariant masses of the incoming and outgoing $q\bar{q}$ pair. In Eq. (3), $\rho(M^2, M'^2)$ is the density

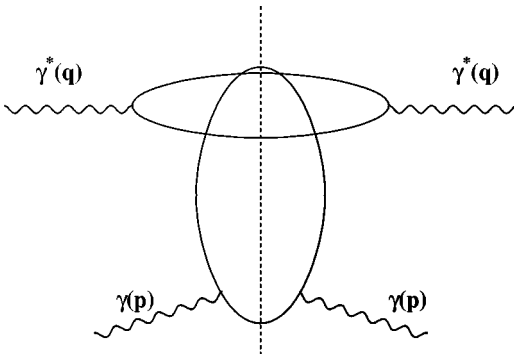


FIG. 5. Diagrammatic representation of the dispersion relation.

matrix of the $q\bar{q}$ states and $\text{Im} A_{(q\bar{q})-\gamma}$ is an imaginary part of the corresponding forward scattering amplitude.

The above formula can be rewritten in the form of a single dispersion relation as follows:

$$F_2^\gamma(W^2, Q^2) = Q^2 \int_0^\infty \frac{dQ'^2}{(Q'^2 + Q^2)^2} \Phi(W^2, Q'^2), \quad (4)$$

where the spectral function is

$$\Phi(W^2, Q'^2) = \frac{1}{4\pi^2\alpha} \int_0^1 d\lambda \int dM^2 \int dM'^2 \delta(Q'^2 - \lambda M'^2 - (1-\lambda)M^2) \rho(M^2, M'^2) \frac{1}{W^2} \times \text{Im} A_{(q\bar{q})-\gamma}(W^2, M^2, M'^2). \quad (5)$$

The center-of-mass energy squared $W^2 = (p+q)^2$ is related to the Bjorken parameter x in the following way:

$$W^2 = Q^2 \left(\frac{1}{x} - 1 \right). \quad (6)$$

One can now separate regions of low and high values of Q'^2 in the integral (4), by noticing that this integral corresponds to the (Generalized) VMD representation of the F_2^γ .

For low values of Q'^2 , $Q'^2 < Q_0^2$, one uses the VMD model. In this approach one assumes that the virtual photon forms a vector meson rather than a pair of well-separated q and \bar{q} . The integrand in the integral on the right-hand side of Eq. (5) defining the spectral function $\Phi(W^2, Q'^2)$ is then given by the following formula:

$$\rho(M^2, M'^2) \frac{1}{W^2} \text{Im} A_{(q\bar{q})-\gamma}(W^2, M^2, M'^2) = \pi\alpha \sum_V \frac{M_V^4}{\gamma_V^2} \sigma_{V\gamma}(W^2) \delta(M^2 - M_V^2) \delta(M'^2 - M_V^2), \quad (7)$$

where M_V is the mass of the vector meson V and $\sigma_{V\gamma}(W^2)$ denotes the $V\gamma$ total cross section. The couplings γ_V^2 can be estimated from the leptonic widths of the vector mesons

$$\frac{\gamma_V^2}{\pi} = \frac{\alpha^2 M_V}{3\Gamma_{e^+e^-}^V}. \quad (8)$$

In Eq. (7) we have included only diagonal transitions between the vector mesons having the same masses. The corresponding spectral function $\Phi^{\text{VMD}}(W^2, Q'^2)$ thus reads

$$\Phi^{\text{VMD}}(W^2, Q'^2) = \sum_V \frac{M_V^4}{4\pi\gamma_V^2} \sigma_{V\gamma}(W^2) \delta(Q'^2 - M_V^2). \quad (9)$$

The resulting VMD contribution to the photon structure function F_2^γ , F_2^{VMD} , is given by the following equation:

$$F_2^{\text{VMD}}(x, Q^2) = \frac{Q^2}{4\pi} \sum_V \frac{M_V^4 \sigma_{V\gamma}(W^2)}{\gamma_V^2 (Q^2 + M_V^2)^2}. \quad (10)$$

In Eq. (10) we only consider mesons with masses $M_V^2 < Q_0^2$. The contribution coming from the region of high values of Q'^2 ($Q'^2 > Q_0^2$) can be related to the photon structure function from the large Q^2 domain. It defines the partonic contribution F_2^{partons} to the structure function F_2^γ , extended to arbitrary low values of Q^2 . For convenience, we adopt the approximation used in Ref. [8] which gives

$$F_2^{\text{partons}}(x, Q^2) = \frac{Q^2}{Q^2 + Q_0^2} F_2^{\text{QCD}}(\bar{x}, Q^2 + Q_0^2), \quad (11)$$

where

$$\bar{x} = \frac{Q^2 + Q_0^2}{W^2 + Q^2 + Q_0^2}. \quad (12)$$

The structure function F_2^{QCD} is taken from the QCD analysis, valid in the large Q^2 region, i.e., it is calculated from the existing parametrizations of the parton distributions for the real photon. Modifications of the QCD contribution are as follows: replacement of the parameter x by \bar{x} defined in Eq. (12), shift of the scale $Q^2 \rightarrow Q^2 + Q_0^2$ and the factor $Q^2/(Q^2 + Q_0^2)$ instead of 1. They introduce power corrections that vanish as $1/Q^2$ and are negligible at large Q^2 . The magnitude of Q_0^2 is set to 1.2 GeV² as in the case of the proton [7,8]. The F_2^{partons} thus defines a contribution to F_2^γ at arbitrary low values of Q^2 .

An elaborated treatment of the partonic contribution to the proton structure function has been developed in Ref. [9], where long and short distance components have been carefully separated. According to that paper the low mass region is dominated by the $q\bar{q}$ pairs with large transverse sizes in the impact parameter space (thus corresponding to the VMD), whereas the QCD part is dominated by pairs of small transverse size.

IV. PARAMETRIZATION OF THE PHOTON STRUCTURE FUNCTION AND OF THE TOTAL PHOTON-PHOTON INTERACTION CROSS SECTIONS

Our representation of the photon structure function $F_2^\gamma(x, Q^2)$ is based on the following decomposition:

$$F_2^\gamma(x, Q^2) = F_2^{\text{VMD}}(x, Q^2) + F_2^{\text{partons}}(x, Q^2), \quad (13)$$

where F_2^{VMD} and $F_2^{\text{partons}}(x, Q^2)$ are defined by Eqs. (10) and (11). A total $\gamma^* \gamma$ cross section in the high energy limit is given by

$$\sigma_{\gamma^* \gamma}(W, Q^2) = \frac{4\pi^2 \alpha}{Q^2} F_2^\gamma(x, Q^2), \quad (14)$$

with $x = Q^2/(Q^2 + W^2)$. The $Q^2 = 0$ (for fixed W) limit of eq. (14) gives the total cross section $\sigma_{\gamma\gamma}(W^2)$ corresponding to

the interaction of two real photons. From Eqs. (13), (10), and (11) we obtain the following expression for this cross section at high energy:

$$\sigma_{\gamma\gamma}(W) = \alpha\pi \sum_{V=\rho, \omega, \phi} \frac{\sigma_{V\gamma}(W^2)}{\gamma_V^2} + \frac{4\pi^2 \alpha}{Q_0^2} F_2^{\text{QCD}}(Q_0^2/W^2, Q_0^2). \quad (15)$$

At large Q^2 the structure function given by Eq. (13) becomes equal to the QCD contribution $F_2^{\text{QCD}}(x, Q^2)$. The VMD component gives the power correction term which vanishes as $1/Q^2$ for large Q^2 . It should be noted that the VMD part contains only a finite number of vector mesons with masses smaller than Q_0^2 .

In the quantitative analysis of the photon structure function and of the total cross sections we have taken the structure function F_2^{QCD} from the leading order (LO) analyses presented in Ref. [19] [Glück-Reya-Vogt (GRV)] and [20] [Glück-Reya-Schienbein (GRS)], with a number of active flavors equal to four. The latter parton parametrization is based on updated data analysis and holds for both virtual and real photons.

The VMD part was estimated using the following assumptions

(1) The numerical values of the couplings γ_V^2 are the same as those used in Ref. [7]. They were estimated from relation (8) which gives the following values:

$$\frac{\gamma_\rho^2}{\pi} = 1.98, \quad \frac{\gamma_\omega^2}{\pi} = 21.07, \quad \frac{\gamma_\phi^2}{\pi} = 13.83. \quad (16)$$

(2) The cross sections $\sigma_{V\gamma}$ are represented as sums of the Pomeron and Reggeon contributions

$$\sigma_{V\gamma}(W^2) = P_{V\gamma}(W^2) + R_{V\gamma}(W^2), \quad (17)$$

where

$$P_{V\gamma}(W^2) = a_{V\gamma}^P \left(\frac{W^2}{W_0^2} \right)^{\lambda_P}, \quad (18)$$

$$R_{V\gamma}(W^2) = a_{V\gamma}^R \left(\frac{W^2}{W_0^2} \right)^{\lambda_R}, \quad (19)$$

with

$$\lambda_R = -0.4525, \quad \lambda_P = 0.0808, \quad (20)$$

and $W_0^2 = 1$ GeV² [24].

(3) Pomeron couplings $a_{V\gamma}^P$ are related to the corresponding couplings $a_{\gamma p}^P$ controlling the Pomeron contributions to the total γp cross sections. We assume the additive quark model and reduce the total cross sections for the interaction of strange quarks by a factor of 2. This gives

$$a_{\rho\gamma}^P = a_{\omega\gamma}^P = \frac{2}{3} a_{\gamma p}^P, \quad (21)$$

$$a_{\phi\gamma}^P = \frac{1}{2} a_{\rho\gamma}^P.$$

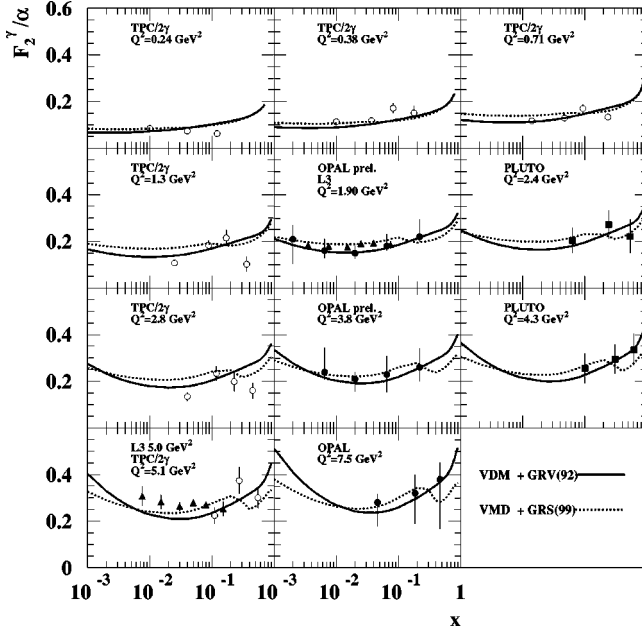


FIG. 6. Comparison of our predictions for F_2^γ/α as a function of x for different values of Q^2 in the low Q^2 region, with experimental results [25–29]. The curves correspond to different LO parametrizations of F_2^{QCD}/α : GRV [19] (solid line) and GRS [20] (dotted line). Error bars correspond to statistical and systematic errors added in quadrature.

(4) Reggeon couplings $a_{V\gamma}^R$ are estimated assuming the additive quark model and the duality (i.e., a dominance of planar quark diagrams). We also assume that the quark couplings to a photon are proportional to the quark charge with the flavor independent proportionality factor. This gives

$$a_{\rho\gamma}^R = a_{\omega\gamma}^R = \frac{5}{9} a_{\gamma p}^R, \quad a_{\phi\gamma}^R = 0. \quad (22)$$

(5) Couplings $a_{\gamma p}^P$ and $a_{\gamma p}^R$ are taken from the fit discussed in Ref. [24] which gave

$$a_{\gamma p}^R = 0.129 \text{ mbarn}, \quad a_{\gamma p}^P = 0.0677 \text{ mbarn}. \quad (23)$$

Since we are using the Regge description of total cross sections $\sigma_{V\gamma}(W)$ our approach can only work for large values of W , $W^2 \gtrsim 2 \text{ GeV}^2$, away from the resonance region.

V. NUMERICAL RESULTS

In this section we compare our results for the real photon structure function $F_2^\gamma(x, Q^2)$ and the two-photon cross sections $\sigma_{\gamma\gamma}(W)$ and $\sigma_{\gamma^*\gamma}(W)$ with corresponding measurements. In some cases our predictions have been extended to the region $W^2 < 2 \text{ GeV}^2$ where the model may not be applicable. Theoretical curves were obtained using two different (LO) parametrizations for the structure function F_2^{QCD} , GRV [19] and GRS [20].

In Fig. 6 we show predictions for the photon structure

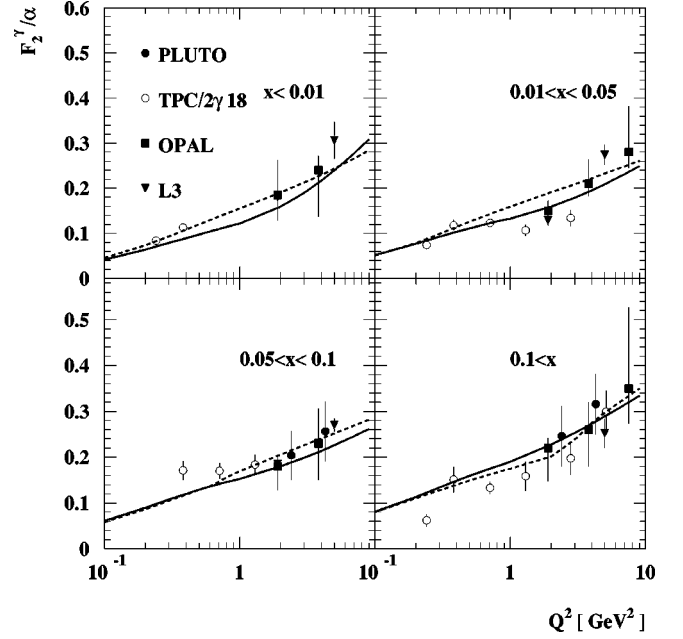


FIG. 7. Comparison of our predictions for F_2^γ/α , as a function of Q^2 in the low Q^2 region, for different intervals of x , with experimental results [25–29]. The curves correspond to different LO parametrization of F_2^{QCD}/α : GRV [19] (solid line) and GRS [20] (dashed line). Curves are plotted for the following values of x (clockwise): 0.0075, 0.0317, 0.0790, and 0.2617. Error bars correspond to statistical and systematic errors added in quadrature.

function based on Eq. (13) plotted as the function of x for different values of Q^2 in the region of small Q^2 . In Fig. 7 the Q^2 dependence of the photon structure function for different values of x is presented.¹ We confront our theoretical results with existing experimental data [25–29]. Measurements of F_2^γ are scarce, especially for low values of Q^2 . However it can be seen that our prediction reproduces well the data independently of the parametrization (GRV or GRS) of F_2^{QCD} used in the model. Irregular behavior of the dashed lines observed in Figs. 6 and 7 at high values of x is connected with the treatment of the charm contribution to F_2^γ in the GRS approach.

In Fig. 8 we compare our predictions with the data on $\sigma_{\gamma\gamma}(W)$. Theoretical curves were obtained from Eq. (15). We show experimental points corresponding to the low energy region ($W \lesssim 10 \text{ GeV}$) [30–32] and the recent preliminary high energy data obtained by the L3, OPAL, and DELPHI Collaborations at CERN e^+e^- collider LEP [33–35]. The representation (15) for the total $\gamma\gamma$ cross section describes the data reasonably well. The result of the calculation based on GRS parametrization of F_2^{QCD} is slightly higher and has a shallower minimum as compared to that based on GRV parametrization. Calculations using the latter give a good description of the shape of the energy dependence of the cross section, although the overall normalization seems to be

¹In both figures the curves are plotted only for $W > 2m_\pi$ which corresponds to the threshold energy in the reaction $\gamma\gamma \rightarrow \text{hadrons}$.

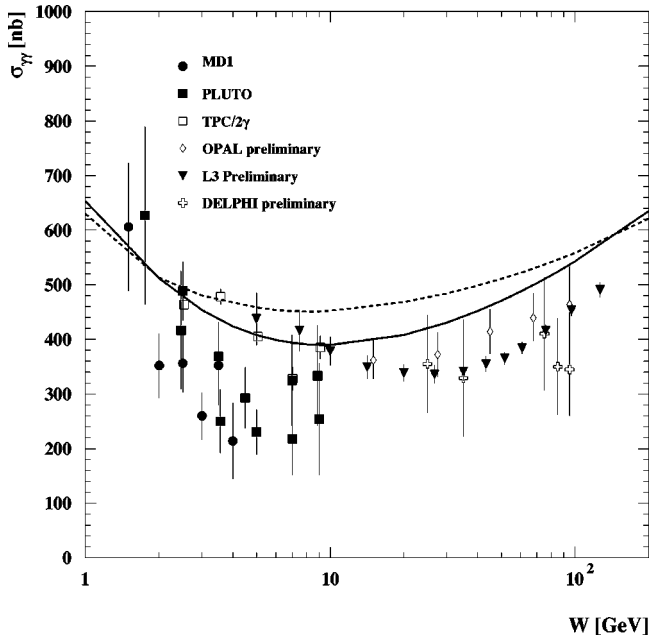


FIG. 8. Comparison of our predictions for $\sigma_{\gamma\gamma}(W)$ based on Eq. (15) with experimental results [30–35]. The curves correspond to different LO parametrizations of F_2^{QCD} : GRV [19] (solid line) and GRS [20] (dashed line). Error bars correspond to statistical and systematic errors added in quadrature.

about 15% too large. It should be stressed that our prediction is essentially parameter free. The magnitude of the cross section is dominated by the VMD component, yet the partonic part is also non-negligible. In particular the latter term is responsible for generating a steeper increase of the total cross section with increasing W than that embodied in the VMD part which is described by the soft Pomeron contribution. The decrease of the total cross section with increasing energy in the low W region is controlled by the Reggeon component of the VMD part [see Eqs. (17), (19), and (20)] and by the valence part of the partonic contribution.

In Fig. 9 we show predictions for the total $\gamma\gamma$ cross section as a function of the total center-of-mass energy W in the wide energy range including the energies that might be accessible in the future linear colliders. In this figure we also show a decomposition of $\sigma_{\gamma\gamma}(W^2)$ into its VMD and partonic components (only GRV parametrization was used in this analysis). At very high energies these two terms exhibit different energy dependence. The VMD part is described by the soft Pomeron contribution which gives the $W^{2\lambda}$ behavior with $\lambda = 0.0808$, Eq. (20). The partonic component increases faster with energy since its energy dependence reflects the increase of $F_2^{\text{QCD}}(\bar{x}, Q_0^2)$ with decreasing \bar{x} generated by the QCD evolution [19,20]. This increase is stronger than that implied by the soft Pomeron exchange. As a result the total $\gamma\gamma$ cross-section, which is the sum of the VMD and partonic components, also exhibits a stronger increase with increasing energy than that of the VMD component. It is, however, milder than the increase generated by the partonic component alone, at least for $W < 10^3$ GeV. This follows from the fact that in this energy range the magnitude of the cross section is still dominated by its VMD component. We found

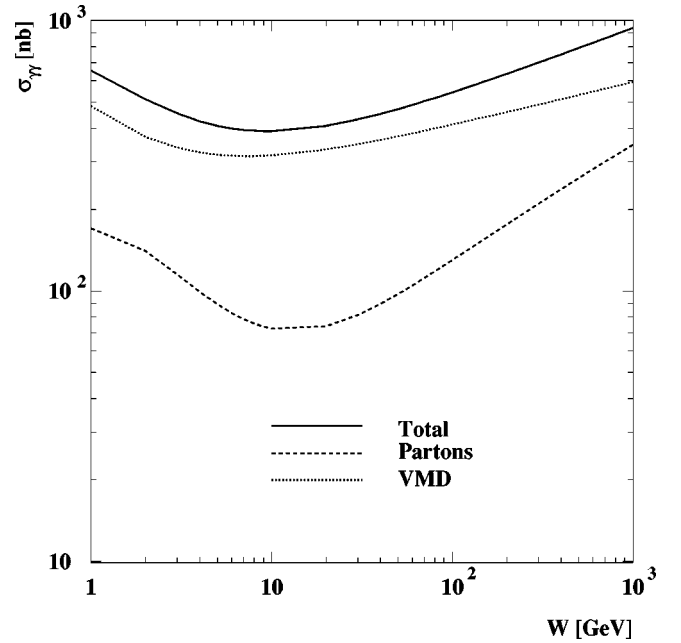


FIG. 9. The total $\gamma\gamma$ cross sections $\sigma_{\gamma\gamma}(W)$ (continuous line) calculated from Eq. (15) and plotted in a wide energy range which includes the region that will be accessible in future linear colliders. Shown separately are the VMD (dotted line) and partonic (dashed line) components of $\sigma_{\gamma\gamma}(W)$. They correspond to the first and the second term on the right-hand side of Eq. (15), respectively. Partonic contribution was obtained using the LO GRV [19] parametrization of F_2^{QCD} .

that for sufficiently high energies W the total $\gamma\gamma$ cross section $\sigma_{\gamma\gamma}(W)$ described by Eq. (15) can be parametrized by the effective power law dependence $\sigma_{\gamma\gamma}(W) \sim (W^2)^{\lambda_{\text{eff}}}$, with λ_{eff} slowly increasing with energy ($\lambda_{\text{eff}} \sim 0.1-0.12$ for $30 \text{ GeV} < W < 10^3 \text{ GeV}$).

In Fig. 10 we show the $\gamma^*\gamma$ cross section for different bins of the center-of-mass energy W plotted versus Q^2 , the virtuality of the γ^* . Our theoretical predictions based on Eq. (14) are compared with measurements by the TPC/2 γ Collaboration [31] and the agreement between the two is very good. In Fig. 11 we show the $\gamma^*\gamma$ cross section for large energies W plotted versus Q^2 (only GRV parametrization was used here). At medium and large Q^2 , $\sigma_{\gamma^*\gamma}$ decreases as $1/Q^2$ (modulo logarithmic corrections) and for very small values ($Q^2 < 10^{-1} \text{ GeV}^2$) it exhibits a flattening behavior.

VI. CONCLUDING REMARKS

We have presented an extension of the representation developed for the nucleon structure function F_2 for arbitrary values of Q^2 , [7,8], onto the structure function of the real photon. This representation includes both the VMD contribution and the QCD component, obtained from the QCD parton parametrizations for the photon, suitably extrapolated to the region of low Q^2 . In the $Q^2=0$ limit the model gives predictions for the total cross section $\sigma_{\gamma\gamma}$ for the interaction of two real photons.

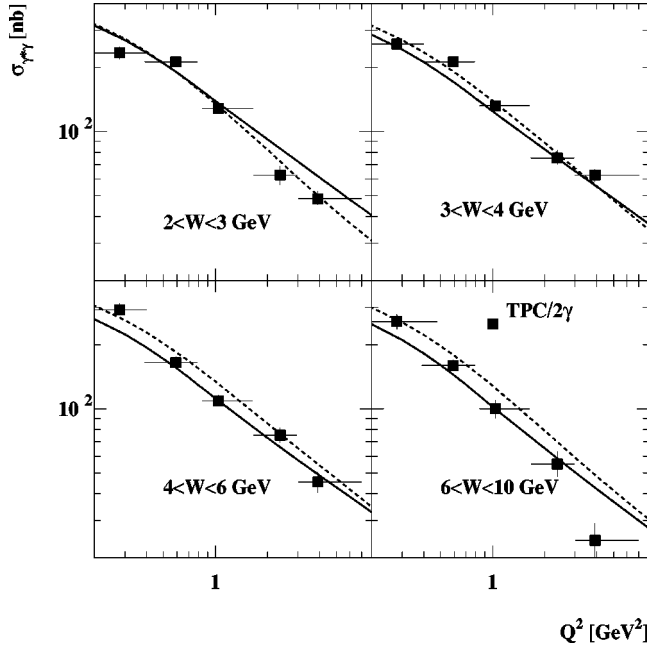


FIG. 10. Comparison of predictions for $\sigma_{\gamma^*\gamma}(W, Q^2)$ in the low Q^2 region based on Eqs. (13), (10), (11), and (14) with experimental results [31]. The curves correspond to the LO parametrizations of F_2^{QCD} : GRV [19] (solid line) and GRS [20] (dashed line), respectively. Error bars correspond to statistical and systematic errors added in quadrature.

We showed that our framework is fairly successful in describing the experimental data on $\sigma_{\gamma\gamma}(W)$ and on $\sigma_{\gamma^*\gamma}(W, Q^2)$ and on the photon structure function F_2^γ at low Q^2 . We also showed that one can naturally explain the fact that the increase of the total $\gamma\gamma$ cross section with increasing CM energy W is stronger than that implied by soft Pomeron exchange. The calculated total $\gamma\gamma$ cross section exhibits an approximate power-law increase with increasing energy W , i.e., $\sigma_{\gamma\gamma}(W) \sim (W^2)^{\lambda_{\text{eff}}}$ with λ_{eff} slowly increasing with en-

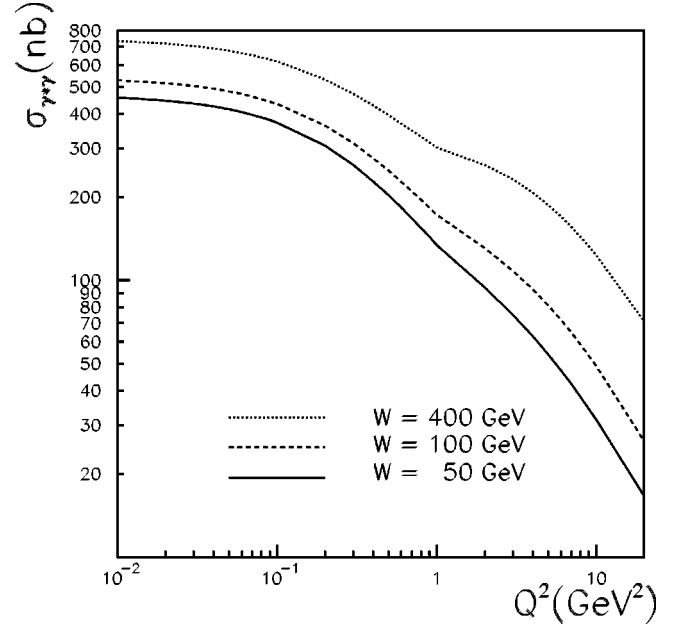


FIG. 11. The total $\gamma^*\gamma$ cross sections $\sigma_{\gamma^*\gamma}(W, Q^2)$ calculated from Eq. (14) as a function of Q^2 for different values of the center-of-mass energy W . Partonic contribution was obtained using the LO GRV [19] parametrization of F_2^{QCD} .

ergy: $\lambda_{\text{eff}} \sim 0.1 - 0.12$ for $30 \text{ GeV} < W < 10^3 \text{ GeV}$. The FORTRAN code calculating F_2^γ and $\sigma_{\gamma\gamma}$ from the model described in this paper is available upon request from: Anna.Stasto@ifj.edu.pl

ACKNOWLEDGMENTS

This research was partially supported by the Polish State Committee for Scientific Research Grant Nos. 2 P03B 089 13, 2 P03B 014 14, 2 P03B 184 10, 2P03B 120 19, 2P03B 051 19 and by the EU Fourth Framework Program ‘‘Training and Mobility of Researchers,’’ Network ‘‘Quantum Chromodynamics and the Deep Structure of Elementary Particles,’’ Contract No. FMRX-CT98-0194.

- [1] E. Witten, Nucl. Phys. **B120**, 189 (1977).
- [2] C. Peterson, T. F. Walsh, and P. M. Zerwas, Nucl. Phys. **B174**, 424 (1980); P. Zerwas, Phys. Rev. D **10**, 1485 (1974).
- [3] H. Abramowicz, M. Krawczyk, K. Charchuła, A. Levy, and U. Maor, Int. J. Mod. Phys. A **8**, 1005 (1993) and references therein.
- [4] Report of the Working Group on $\gamma\gamma$ Physics, P. Aurenche and G. A. Schuler (convenors), Proceedings of the Workshop on Physics at LEP2, CERN yellow report 96-01, edited by G. Altarelli, T. Sjöstrand, and P. Zwirner; hep-ph/9601317.
- [5] M. Krawczyk, Acta Phys. Pol. B **28**, 2659 (1997); M. Krawczyk, A. Zembrzuski, and M. Staszal, hep-ph/9806291; an extended version of this report is in IFT 99-15; P. Nisius, Phys. Rep. **332**, 165 (2000).
- [6] T. H. Bauer *et al.*, Rev. Mod. Phys. **50**, 261 (1978), and references therein.

- [7] J. Kwieciński and B. Badełek, Z. Phys. C **43**, 251 (1989).
- [8] B. Badełek and J. Kwieciński, Phys. Lett. B **295**, 263 (1992).
- [9] A. D. Martin, M. G. Ryskin, and A. M. Stasto, Eur. Phys. J. C **7**, 643 (1999); Nucl. Phys. B (Proc. Suppl.) **74**, 121 (1999).
- [10] E. Gotsman, A. Levy, and U. Maor, Z. Phys. C **40**, 117 (1988).
- [11] G. A. Schuler, Comput. Phys. Commun. **108**, 279 (1998).
- [12] A. Donnachie, H. G. Dosch, and M. Rueter, Phys. Rev. D **59**, 074011 (1999).
- [13] J. R. Forshaw and J. K. Storrow, Phys. Rev. D **46**, 4955 (1992); Phys. Lett. B **278**, 193 (1992).
- [14] G. A. Schuler and T. Sjöstrand, Z. Phys. C **73**, 677 (1997).
- [15] A. Donnachie, H. G. Dosch, and M. Rueter, Eur. Phys. J. C **13**, 141 (2000).
- [16] A. Corsetti, R. M. Godbole, and G. Pancheri, Phys. Lett. B **435**, 441 (1998) and references therein; R. M. Godbole, A. Grau, and G. Pancheri, Nucl. Phys. B (Proc. Suppl.) **82**, 246 (2000); IISC-CTS-8-99, hep-ph/9912395.

- [17] A. Donnachie and S. Soldner-Rembold, FREIBURG-EHEP-2000-01, hep-ph/0001035.
- [18] E. Gotsman *et al.*, Eur. Phys. J. C **14**, 511 (2000).
- [19] M. Glück, E. Reya, and A. Vogt, Phys. Rev. D **46**, 1973 (1992).
- [20] M. Glück, E. Reya, and I. Schienbein, Phys. Rev. D **60**, 054019 (1999).
- [21] A. M. Cooper-Sarkar, R. C. E. Devenish, and A. De Roeck, Int. J. Mod. Phys. A **13**, 3385 (1998).
- [22] A. Vogt, in Proceedings of the International Conference on the Structure and Interactions of the Photon, PHOTON 99, Freiburg, 1999 [Nucl. Phys. B (Proc. Suppl.) **82**, 394 (2000)]; E. Accomando *et al.*, Phys. Rep. **299**, 21 (1998).
- [23] G. A. Schuler and T. Sjöstrand, Z. Phys. C **68**, 607 (1995).
- [24] A. Donnachie and P. V. Landshoff, Phys. Lett. B **296**, 227 (1992).
- [25] PLUTO Collaboration and Ch. Berger *et al.*, Phys. Lett. **142B**, 111 (1984); Nucl. Phys. **B281**, 365 (1987).
- [26] TPC/2 γ Collaboration, H. Aihara *et al.*, Z. Phys. C **34**, 1 (1987).
- [27] L3 Collaboration, M. Acciarri *et al.*, Phys. Lett. B **436**, 403 (1998).
- [28] OPAL Collaboration, Physics Note PN389 (1999).
- [29] OPAL Collaboration, K. Ackerstaff *et al.*, Z. Phys. C **74**, 33 (1997).
- [30] PLUTO Collaboration, Ch. Berger *et al.*, Phys. Lett. **149B**, 421 (1984); Z. Phys. C **26**, 353 (1984).
- [31] TPC/2 γ Collaboration, H. Aihara *et al.*, Phys. Rev. D **41**, 2667 (1990).
- [32] MD-1 Collaboration, S. E. Baru *et al.*, Z. Phys. C **53**, 219 (1992).
- [33] L3 Collaboration, G. Passaleva, talk presented at the IX Lomonosov Conference on Elementary Particle Physics, Moscow, 1999.
- [34] OPAL Collaboration, G. Abbiendi *et al.*, Eur. Phys. J. C **14**, 199 (2000).
- [35] DELPHI Collaboration, N. Zimin, in *Proceedings of the International Conference on the Structure and Interactions of the Photon, PHOTON 99*, Freiburg, 1999 [Nucl. Phys. B (Proc. Suppl.) **82**, 139 (2000)].